Optically active centers in Eu implanted, Eu *in situ* doped GaN, and Eu doped GaN quantum dots

L. Bodiou,[1] A. Braud,[1,a)] J.-L. Doualan,[1] R. Moncorgé,[1] J. H. Park,[2] C. Munasinghe,[2] A. J. Steckl,[2] K. Lorenz,[3] E. Alves,[3] and B. Daudin[4]
[1]*Centre de Recherche sur les Ions, les Matériaux et la Photonique (CIMAP), CNRS-CEA-ENSICAEN, Université de Caen, UMR 6252, 14050 Caen, France*
[2]*University of Cincinnati, Cincinnati, Ohio 45221-0030, USA*
[3]*Instituto Tecnologico e Nuclear, Estrada Nacional 10, PT-2685-953 Sacavém, Portugal*
[4]*INAC SP2M/PSC, CEA-Grenoble, 17 rue des Martyrs, 38054 Grenoble Cedex 9, France*

(Received 17 June 2008; accepted 29 December 2008; published online 18 February 2009)

A comparison is presented between Eu implanted and Eu *in situ* doped GaN thin films showing that two predominant Eu sites are optically active around 620 nm in both types of samples with below and above bandgap excitation. One of these sites, identified as a Ga substitutional site, is common to both types of Eu doped GaN samples despite the difference in the GaN film growth method and in the doping technique. High-resolution photoluminescence (PL) spectra under resonant excitation reveal that in all samples these two host-sensitized sites are in small amount compared to the majority of Eu ions which occupy isolated Ga substitutional sites and thus cannot be excited through the GaN host. The relative concentrations of the two predominant host-sensitized Eu sites are strongly affected by the annealing temperature for Eu implanted samples and by the group III element time opening in the molecular beam epitaxy growth. Red luminescence decay characteristics for the two Eu sites reveal different excitation paths. PL dynamics under above bandgap excitation indicate that Eu ions occupying a Ga substitutional site are either excited directly into the $^5D_0$ level or into higher excited levels such as $^5D_1$, while Eu ions sitting in the other site are only directly excited into the $^5D_0$ level. These differences are discussed in terms of the spectral overlap between the emission band of a nearby bound exciton and the absorption bands of Eu ions. The study of Eu doped GaN quantum dots reveals the existence of only one type of Eu site under above bandgap excitation, with Eu PL dynamics features similar to Eu ions in Ga substitutional sites. © *2009 American Institute of Physics*. [DOI: 10.1063/1.3078783]

I. INTRODUCTION

Rare earth (RE) doped III-V semiconductors have attracted large research interest because of their potential applications in optoelectronics such as electroluminescent devices[1,2] and novel semiconductor lasers.[3,4] They offer the opportunity of combining the electrical excitation of the host material and the remarkable optical properties of RE ions. In this context, the red luminescence arising from the $^5D_0 \rightarrow {}^7F_2$ intra-4*f* shell transition of trivalent Eu^{3+} ions is very promising. Several reports have already shown the prominence of Eu^{3+} luminescence in GaN.[5–9] The excitation mechanisms leading to the luminescence of Eu^{3+} ions in III-N compounds remain, however, unclear. One of the major issues is that the incorporation, excitation, and luminescence of Eu^{3+} ions might change depending on the doping method, whether it is performed *in situ* during growth or postgrowth by ion implantation. The purposes of this work are to present a comparison between Eu doped GaN samples grown by very different doping and growth methods [implantation, *in situ* doping, and Eu *in situ* doped quantum dots (QDs)] and to show recurrent features, which appear to be intrinsic to this type of system for all types of growth conditions. Little or no analysis has been done to date to compare RE doped GaN coming from different groups and grown with different methods. A photoluminescence (PL) excitation study for a below bandgap excitation in Er doped GaN reported[10] some similarities between ion-implanted and *in situ* doped GaN samples in case of Er resonant excitation. Another comparison between Er doped GaN prepared by metal-organic molecular beam epitaxy (MOMBE) and solid-source MBE (SSMBE) shows green PL signal only from SSMBE samples.[11]

Despite the lack of comparison between RE implanted and *in situ* doped GaN samples, interesting results have been obtained for both types of samples. For ion-implanted samples, the GaN growth using either MBE or metalorganic chemical vapor deposition (MOCVD) prior to ion implantation appears to have little effect on the subsequent luminescence properties of the RE ions embedded in the host matrix.[12] On the other hand, the annealing temperature has been shown to be a crucial parameter in the activation of the RE luminescence in RE implanted GaN.[13]

As far as RE incorporation sites are concerned, it has been reported[14,15] that under above bandgap excitation the Eu luminescence at 10 K arises predominantly from two different Eu sites in implanted GaN:Eu samples annealed at 1100 °C and above. The existence of multiple Eu sites was also suggested for MBE samples characterized by conventional PL.[16,17] A study[18] of stimulated emission in GaN:Eu *in*

a)Electronic mail: alain.braud@ensicaen.fr.

TABLE I. Growth conditions for GaN:Eu samples produced by ion implantation.

Implanted GaN:Eu	Fluence (at./cm^2)	Implantation energy (keV)	Implantation temperature (K)	Capping layer	Annealing temperature (°C)	Annealing time (min)
I-1000	1×10^{15}	300	300		1000	2
I-1100	1×10^{15}	300	300	AlN (10 nm)	1100	20
I-1200	1×10^{15}	300	300	AlN (10 nm)	1200	20
I-1300	1×10^{15}	300	300	AlN (10 nm)	1300	20

situ doped MBE samples identified two main sites: Eu_x—emitting at ~620 nm, producing stimulated emission and exhibiting a fast decay time constant; Eu_y—emitting at 621 nm, producing only spontaneous emission and having a slower decay time constant. These results clearly indicate the need for a comprehensive study of Eu sites in GaN and their relationship to emission mechanisms.

We report here a comparison of site dependent emission characteristics using high-resolution PL spectra between *in situ* implanted Eu doped GaN thin films and Eu doped GaN QDs. High-resolution PL spectra were investigated for all samples as a function of the excitation power density as well as the PL lifetime characteristics. The results show the existence of a common Eu site in implanted and *in situ* samples which is associated with the Ga substitutional site. Differences between the common Eu site and other Eu sites are further discussed in relation to the growth and doping techniques.

II. SAMPLES AND MEASUREMENTS

Three types of GaN:Eu samples were investigated. A first set of four samples consists of GaN epilayers grown by MOCVD on *c*-plane sapphire at 1090 °C following a low temperature GaN buffer layer. For three of the four samples the GaN growth was followed by the epitaxial deposition at 1160 °C of a 10 nm thick AlN capping layer. These samples were subsequently implanted with Eu ions. Implantation and annealing conditions are summarized in Table I. Europium ions were implanted normally either through the AlN cap (samples I-1100, I-1200, and I-1300) or directly into the GaN (I-1000) at 25 °C using an energy of 300 keV and a fluence of 1×10^{15} at./cm^2. The AlN cap allowed the implanted samples to be annealed for 20 min at high temperatures ranging from 1100 up to 1300 °C in a conventional tube furnace with a moderate N_2 overpressure (4 bars). Rutherford backscattering (RBS) depth profiling showed for all samples a maximum concentration of 0.2 at. % at ~70 nm depth. A second set of samples (Table II) was grown by MBE with the *interrupted growth epitaxy* (IGE) technique,[19,20] for which the shutters of group III elements (Ga and Eu) are open ("on") for a part of the cycle and close ("off") for the rest of the time. The group V is on throughout the entire IGE cycling time. The goal of the IGE technique is to prevent the formation of GaN islands on the substrate surface that deteriorates the material crystallinity. Secondary ion mass spectrometry (SIMS) measurements indicate that Eu concentrations in the samples range between 0.3 and 0.4 at. % (Table II).

A third type of sample consisted of Eu doped GaN QDs embedded in an AlN matrix. The sample was grown on 1-μm-thick AlN pseudosubstrate deposited by MOCVD on *c*-sapphire. After a standard chemical degreasing procedure and acid cleaning, it was fixed onto a molybdenum sample holder and introduced in a MBE chamber equipped with Al, Ga, and Eu effusion cells and a radio-frequency plasma cell to produce monoatomic nitrogen. The GaN QDs were grown at a substrate temperature of about 720 °C following the Stranski–Krastanov growth mode, i.e., the QDs appear after the deposition of about 2.5 GaN monolayers (MLs). The growth conditions were controlled with reflection high-energy electron diffraction, which allows *in situ* monitoring of the QD formation. During the growth of GaN, the Eu shutter was opened in order to dope the material. The amount of GaN nominally deposited was about 5 MLs. Next, the QDs were capped by about 10 nm of undoped AlN in order to recover a smooth surface. This process was repeated to achieve a superlattice of 80 QD planes. From the chosen growth conditions the Eu content inside the sample was estimated to be around 1%–2%, mostly incorporated in GaN, while the content in AlN barrier is negligible.[21]

TABLE II. Growth conditions and Eu concentrations for GaN:Eu samples produced by interrupted growth MBE.

	Shutter open or close time during one cycle				
MBE GaN:Eu	Group III on (min)	Group III off (min)	Group V on (min)	No. of cycles repeated	Concentration (SIMS) (at. %)
M-60	60	0	60	1	0.4
M-30	30	5	35	2	0.3
M-20	20	5	25	3	0.35
M-15	15	5	20	4	0.3
M-10	10	5	15	6	0.4
M-5	5	5	10	12	0.35

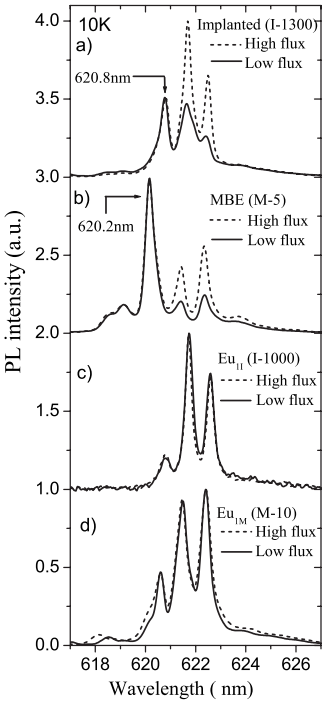

FIG. 1. Eu PL spectra recorded at 10 K ($^5D_0 \rightarrow {}^7F_2$ transition) under above bandgap excitation (λ_{exc}=325 nm) for low and high photon fluxes ($\phi_{low} \approx 10^{18}$ s^{-1} cm^{-2} and $\phi_{high} \approx 2\times10^{20}$ s^{-1} cm^{-2}): (a) implanted sample I-1300; (b) *in situ* doped sample M-5; (c) implanted sample I-1000; and (d) *in situ* doped sample M-10.

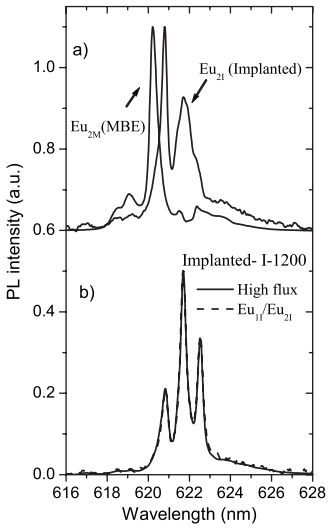

FIG. 2. (a) PL spectra of Eu_2 sites in MBE (Eu_{2M}) and implanted samples (Eu_{2I}) recorded with 514 nm excitation in samples M-5 and I-1300, respectively. (b) Comparison between PL spectrum recorded with sample I-1200 (ϕ=4.3×10^{20} s^{-1} cm^{-2}) and an adequate combination of Eu_{1I} and Eu_{2I} spectra ($0.7Eu_{1I}+0.3Eu_{2I}$).

The GaN:Eu samples were mounted in a closed-cycle helium cryostat and cooled down to 10 K. PL studies were performed by exciting the GaN:Eu samples with a HeCd laser (λ_{exc}=325 nm) or an argon ion laser (λ_{exc}=514 or 488 nm). Visible luminescence was recorded using a 0.75 m monochromator. The monochromator resolution was below 0.1 nm for all spectra. For luminescence decay measurements, a frequency tripled- or quadrupled-Nd doped yttrium aluminum garnet (YAG) pulsed laser source (λ_{exc}=355 or 266 nm) was used along with a detection setup having a time response of about 80 ns.

III. RESULTS AND ANALYSIS

A. Two main Eu sites in Eu implanted and *in situ* doped GaN samples

Figures 1(a) and 1(b) show the PL spectra of I-1300 and M-5 samples at two different excitation power density levels. Three peaks appear in the 622–624 nm range in both cases. The spectra are normalized to the PL intensity at the dominant peak wavelength (620.8 nm for sample I-1300 and 620.2 nm for sample M-5) in order to emphasize the differences between the spectral shapes. For both implanted and MBE GaN:Eu samples, as the excitation photon flux goes from low ($\phi_{low} \approx 1\times10^{18}$ s^{-1} cm^{-2}) to high ($\phi_{high} \approx 2\times10^{20}$ s^{-1} cm^{-2}), the two long wavelength peaks increase in prominence compared to the shorter wavelength peak. This PL dependence on flux suggests that there are two different Eu sites in the GaN host. A similar change in the spectra is observed in all implanted and MBE samples except for the PL spectra of samples I-1000 and M-10 displayed in Figs. 1(c) and 1(d) for which almost no change occurs when the photon flux is increased over the same range. This result indicates that for these two samples, there is only one specific Eu^{3+} site, which we will refer to as Eu_{1I} and Eu_{1M} for implanted and MBE samples, respectively. It is important to note that we have found other minor sites both in implanted and MBE grown GaN:Eu samples under above bandgap excitation. In most cases these sites represent only a small fraction in comparison to the two major sites that are discussed in this paper.

PL spectra of all the other samples measured at low or high photon flux such as the ones displayed in Fig. 1 appear to be linear combinations of the Eu_1 spectra presented in Figs. 1(c) and 1(d) with another spectrum related to a second type of Eu site which we will refer to as Eu_2 site. The PL spectra of this Eu_2 site (Eu_{2I} and Eu_{2M} for implanted and MBE samples, respectively) shown in Fig. 2(a) can be selectively recorded by exciting the samples at 514 nm. This below bandgap excitation wavelength excites only this particular Eu_2 site in all samples because of a much larger effective excitation cross section of this site at this wavelength compared to the Eu_1 site. The same Eu_{2I} spectrum as displayed in Fig. 2(a) is obtained in all implanted samples. Similarly, the Eu_{2M} spectrum in Fig. 2(a) is obtained in all MBE samples. A typical comparison between an above bandgap excited Eu PL spectrum (ϕ=4.3×10^{20} s^{-1} cm^{-2}) and its reconstruction using the spectral signatures of Eu_1 and Eu_2 sites is illustrated in Fig. 2(b) for sample I-1200 showing a very good agreement.

The change in PL spectral shape with the excitation photon flux illustrated in Fig. 1 is remarkable. The fact that different Eu PL spectra in GaN can be found in the literature could be explained for some of them not so much by a multiplicity of Eu sites which would depend on the sample growth and doping conditions but rather by the PL excitation conditions which change from one study to another. At low

photon flux the PL intensity of Eu_2 sites is dominant. At higher photon flux the Eu_2 luminescence saturates while the Eu_1 sites luminescence continues to increase.[14] In other words, the above bandgap effective excitation cross section related to the Eu_2 site is larger than for the Eu_1 site in both implanted and MBE samples. Above bandgap excitation is commonly described as being mediated by a nearby carrier trap before reaching the Eu ion. Indeed, following an above bandgap excitation, free carriers might be captured by defects or impurities forming trapped electron-hole pairs. The electron-hole pair can then transfer its energy nonradiatively to a nearby RE ion.[22] The carrier trap can be simply induced by the incorporated RE ions forming isoelectronic traps or it may originate from a more complex center where the RE ion is coupled to a structural defect or a different chemical impurity. Density functional theory calculations show that carrier traps are unlikely to be directly induced by the RE substitution in GaN.[23] Therefore, Eu_1 and Eu_2 sites might be part of complexes involving defects or impurities. The fact that Eu_2 sites are more efficiently excited could imply that the coupling between the carrier trap and Eu_2 site is stronger than for the Eu_1 site. A possible explanation would be that the local defect inducing the carrier trap is located further away from the actual Eu site in the case of Eu_1 ions for which the Eu local site symmetry is much less perturbed. In this case, the carrier trap could be located, for instance, in the second or third nearest-neighbor shell. This assumption is supported by the fact that the Eu_1 spectra [Figs. 1(c) and 1(d)] of implanted and MBE GaN samples are strikingly similar, while the Eu_{2I} and Eu_{2M} spectra [Fig. 2(a)] are clearly different. The similarity between the Eu_1 spectra strongly suggests that the Eu_1 incorporation site does not depend on the Eu doping method or the GaN growth technique and, therefore, it is likely a Ga substitutional site. To verify this hypothesis, we performed a resonant excitation of Eu ions at 471.3 nm ($^7F_0 \rightarrow {}^5D_2$) depicted in Fig. 3(a) for an implanted sample (I-1300) and in Fig. 3(b) for a MBE sample (M-20) at 10 K. The resonant PL spectrum appears to be identical to the Eu_1 PL spectrum obtained in sample I-1000 and sample M-10 under above bandgap excitation. The vast majority of Eu ions contributing to the resonant PL spectrum is, in fact, located in Ga substitutional sites as revealed by RBS experiments[24] and confirmed by *ab initio* calculations.[25] Another evidence that Eu_1 ions occupy Ga substitutional sites in all samples is that a Ga substitutional site has a C_{3v} symmetry in GaN. In C_{3v} symmetry the $^7F_2$ terminal level ($J=2$) is expected to be split into three Stark components, which is consistent with the three lines observed in the Eu_1 $^5D_0 \rightarrow {}^7F_2$ PL spectrum.

In contrast, the differences between Eu_{2I} and Eu_{2M} spectra [Fig. 2(a)] indicate that the Eu_2 incorporation site differs in implanted and MBE samples. These differences could be explained by a local defect in close proximity distorting the local Eu symmetry and enabling a strong coupling between the carrier trap and the Eu_2 ions. However, the number of complexes involving Eu_2 ions appears to be small. The Eu PL spectrum under resonant excitation shown in Fig. 3 for samples I-1300 and M-20 reveals that the PL contribution from Eu_2 ions is negligible. This result is even more remarkable since samples I-1300 and M-20 are the two samples for which the above bandgap excitation leads to the strongest contribution from Eu_2 ions as will be shown later in the text. Spectra in Fig. 3 thus strongly support the idea of a small number of Eu_2 ions compared to the vast majority of Eu ions sitting in Ga substitutional sites. Similar results have been previously reported in Er doped GaN samples showing that Er indirect excitation involves erbium-carrier trap complexes in small amount compared to isolated Er centers.[26] Another possible way of assessing the multiplicity of incorporation sites in Eu doped compounds consists in the study of the $^5D_0 \rightarrow {}^7F_0$ transition which exhibits only one line for each Eu incorporation site. Unfortunately, this transition, which is forbidden, is usually very weak and could not be observed in the samples used in this study by pumping either resonantly or nonresonantly.

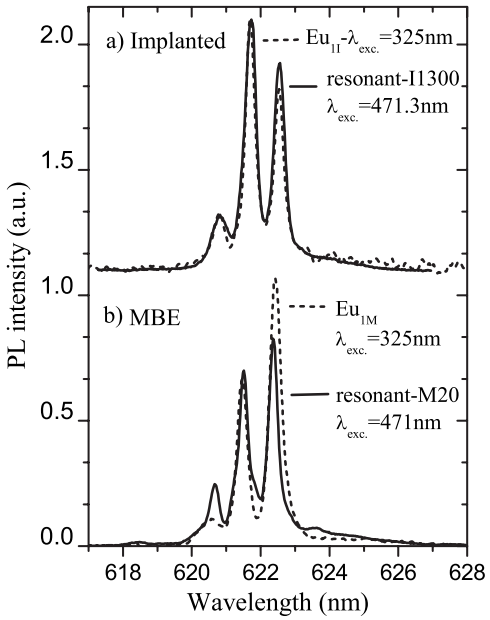

FIG. 3. Comparison between Eu_1 spectrum (above bandgap excitation, $\lambda_{exc}=325$ nm) and Eu spectrum under resonant excitation at 471 nm ($^7F_0 \rightarrow {}^5D_2$ transition): (a) implanted sample I-1300 and (b) MBE sample M-20.

B. Relative concentrations of both Eu sites

In order to assess the number of Eu_1 sites compared to the number of Eu_2 sites, the excitation photon flux was increased so as to reach the saturation regime of the luminescence arising from Eu_2 and Eu_1 ions. The expected dependence of the Eu luminescence as a function of the excitation photon flux is as follows:[14]

$$I_{1,2} \alpha N_{1,2} \times [1 + (\sigma_{1,2} \times \tau_{1,2} \times \phi)^{-1}]^{-1}, \quad (1)$$

where N_1 and N_2 are the Eu_1 and Eu_2 concentrations, σ_1 and σ_2 are the Eu_1 and Eu_2 effective excitation cross sections, ϕ is the photon flux, and τ_1 and τ_2 are the $^5D_0$ level lifetimes for Eu_1 and Eu_2 ions, respectively. An example of luminescence saturation curves recorded at 12 K is shown in Fig. 4(a) for implanted sample I-1200 at different emission wavelengths and also in Fig. 4(b) for MBE samples M-5 and M-20. As expected, the PL signals at 620.8 nm for implanted samples and 620.2 nm for MBE samples arise predominantly

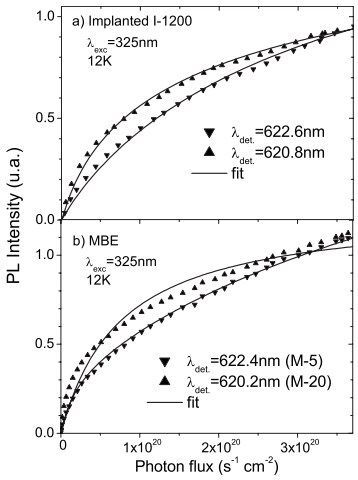

FIG. 4. (a) PL saturation curves at 12 K under above bandgap excitation (λ_{exc}=325 nm) in implanted sample I-1200 at 622.6 and 620.8 nm. (b) PL saturation curves at 12 K (λ_{exc}=325 nm) in MBE samples M-5 at 622.4 nm and M-20 at 620.2 nm.

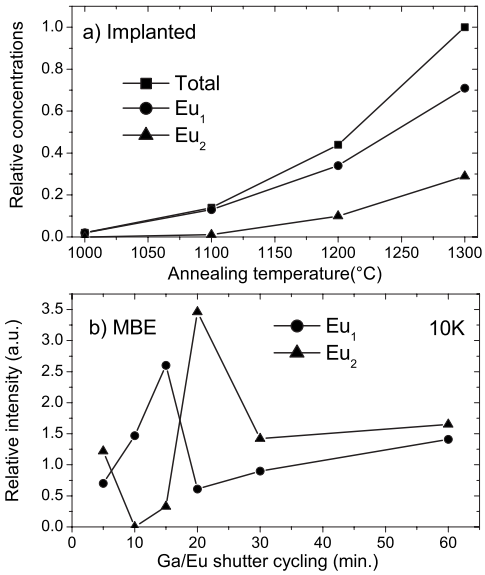

FIG. 5. (a) Relative concentrations of Eu_1 and Eu_2 centers in implanted samples derived from the extrapolation of PL saturation curves as a function of annealing temperature. (b) $^5D_0 \rightarrow {}^7F_2$ transition PL relative intensity of Eu_1 and Eu_2 centers in IGE *in situ* doped GaN samples at 10 K vs the opening time of group III elements (λ_{exc}=325 nm, $\phi = 3 \times 10^{19}$ s^{-1} cm^{-2}).

from Eu_2 ions and thus saturate faster than at longer wavelengths which are characteristic of Eu_1 ions (622.6 nm for implanted and 622.4 nm for MBE samples).

Equation (1) shows that for a very large photon flux value ($\phi \gg \sigma_{1,2} \cdot \tau_{1,2}$) the luminescence intensity becomes proportional to the concentration of Eu ions. By obtaining this value of the luminescence intensity under complete saturation it then becomes possible to know the relative concentrations of different Eu sites in a same sample. However, in order to have a convincing estimate of the relative concentrations of these Eu species several steps in the data treatment must be taken. First, it is necessary to extrapolate for a very large photon flux the fitting curves displayed in Fig. 4 which were obtained by adjusting Eq. (1) to the experimental saturation curves. This procedure is valid only if the fitting curves match accurately the experimental data [Fig. 4(a)]. Another issue is that the luminescence saturation curve recorded at a specific wavelength, as shown in Fig. 4(a) for sample I-1200, encompasses, in fact, contributions from the two species. It is thus necessary to discriminate between contributions from the two species using the known Eu_1 and Eu_2 spectra [Fig. 2(b)]. Moreover, in order for the luminescence intensity to reflect the concentration of one species relative to the other, the luminescence intensity recorded at a specific wavelength has to be corrected in order to reflect the intensity of the entire $^5D_0 \rightarrow {}^7F_2$ intra-4*f* shell transition. For instance, in the *in situ* doped samples, the luminescence intensity recorded around 622.4 nm within the 4 Å spectral window used in Fig. 4(b) represents 19.5% of the total $^5D_0 \rightarrow {}^7F_2$ intra-4*f* shell transition for Eu_{1M} ions, while it only represents 4% of the transition intensity for Eu_{2M} ions. Once deconvolution between overlapping spectra and intensity corrections are performed, it is possible to derive the relative concentrations of each Eu site from the intensities reached by each type of Eu centers upon complete saturation. Figure 5(a) gives the relative concentrations of both types of Eu sites in implanted samples as a function of annealing temperature. To obtain a reliable comparison between samples it is crucial that the excitation and collection geometry remain unchanged while investigating one sample after another.

From the data of Fig. 5(a), it is clear that for all implanted samples the annealing temperature plays a major role in the activation of Eu_{2I} ions for as the annealing temperature is raised the number of optically active Eu_{2I} ions steadily increases. As mentioned earlier, for an annealing temperature of 1000 °C (sample I-1000) there is no luminescence from Eu_{2I} ions. This suggests that the annealing treatment removes quenching centers which otherwise prevent Eu_{2I} ions from emitting or from being excited. Moreover, the raising annealing temperature not only enables the luminescence from more Eu_{2I} ions, but the number of optically active Eu_{1I} ions also increases by a factor of 35 between 1000 and 1300 °C as depicted in Fig. 5(a).

We mentioned earlier that the absence of luminescence from Eu_{2I} ions in the resonant spectrum in Fig. 3(a) indicates that the number of Eu_{2I} ions is very small compared to the vast majority of Eu ions sitting in Ga substitutional sites. Interestingly, one can see in Fig. 5(a) that for an annealing temperature of 1300 °C (sample I-1300) the number of Eu_{1I} ions is only twice the number of Eu_{2I} ions. Therefore, the number of Eu_{1I} ions must also be small compared to the total amount of Eu ions. This result shows that only a small part of Eu ions in a Ga substitutional site can be excited through the host and, thus, be labeled as Eu_1 ions. In other words, the traps which bind excitons close to Eu_1 ions are not induced by the substitution of Eu ions to Ga atoms but rather, as mentioned previously, by local defects or impurities close to substitutional Eu ions. This result is also verified in the case of *in situ* doped samples and will be illustrated here in the case of sample M-5. Following the same data treatment as for implanted samples, the luminescence saturation curves of sample M-5 recorded at several emission wavelengths are adjusted with Eq. (1) as displayed in Fig. 4(b). The fitting procedure reveals that in sample M-5 the amount of Eu_{2M}

ions is three times larger than the number of Eu_{1M} centers. Yet, under resonant excitation the luminescence from Eu_{2M} ions is too small to be seen in the resonant spectrum displayed in Fig. 3(b). One can see again that the number of Eu_{2M} and hence the number of Eu_{1M} centers are much smaller than the rest of Eu ions which occupy Ga substitutional sites and cannot be excited by host sensitization. All these results indicate that at least two types of Eu ions in Ga substitutional sites exist in Eu doped GaN samples: a vast majority of isolated Eu ions which can only be excited resonantly and a small amount of substitutional sites (Eu_1 ions) which can be excited via nearby carrier traps.

Unlike the results presented in Fig. 5(a) for implanted samples, the determination of the relative concentrations of Eu_{1M} and Eu_{2M} ions in *in situ* samples was not possible for all samples since some luminescence saturation curves could not be accurately adjusted with Eq. (1). An example of a tentative fit is given in Fig. 5(b) for sample M-20 at 10 K. The reason for this poor adjustment lies in the model describing the excitation pathway itself. The rather simple rate equation model used to derive Eq. (1) makes use of an effective excitation cross section which encompasses all the steps of the excitation path into one single parameter. For some *in situ* samples, the model needs to be refined by precisely describing the free carrier creation, the subsequent carrier trapping, and the energy transfer from the bound exciton to the RE ion. Such a model is under development and will be presented in an upcoming publication. Nevertheless, some conclusions can be drawn from looking at the PL spectra of all the MBE samples grown by the IGE technique provided that the PL spectra are recorded in the same excitation conditions. For all MBE samples like for implanted samples, we were able to discriminate between contributions from the two major sites using the high-resolution PL Eu_{1M} and Eu_{2M} spectra displayed in Figs. 1(d) and 2(a), respectively. Figure 5(b) presents the relative intensity of the $^5D_0 \rightarrow {}^7F_2$ transition for both sites in IGE samples at 10 K. For IGE *in situ* doped samples the difference between samples lies in the opening time of group III elements during growth. Figure 5(b) shows that the IGE cycling time appears to affect the PL of Eu_{2M} ions and Eu_{1M} ions in such a way to create an anticorrelation between the luminescence intensities of Eu_{1M} and Eu_{2M} ions. A similar anticorrelation between both Eu site emissions was recently reported by Park and Steckl[18] for the same type of IGE samples using lower resolution spectra obtained by exciting the samples with a Xe lamp which gives less PL signal than using a laser. The results displayed in Fig. 5(b) indicate that, unlike what is observed in implanted samples, a competition seems to take place between Eu_{1M} and Eu_{2M} ions in the IGE samples. This competition associated with the IGE cycling time directly affects either the creation of Eu_{1M} and Eu_{2M} centers during growth or the activation of these centers. This latter hypothesis implies that the IGE cycling time is not so much decisive for the RE doping itself as for the creation of the necessary nearby carrier traps which enable the indirect excitation of RE ions. In this sense, the opening time of group III elements during growth could promote the formation of specific carrier traps rather than others. For instance, a cycling time of 15 min (sample M-15) appears to favor the creation of carrier traps enabling the excitation of Eu ions in Ga substitutional sites (Eu_{1M} ions).

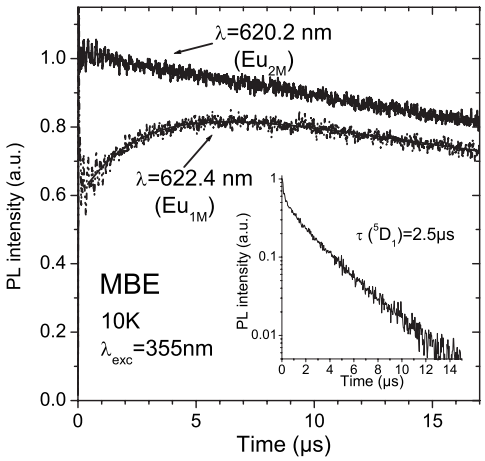

FIG. 6. Initial stage of the time dependent PL recorded at 620.2 nm (Eu_2 site) and 622.4 nm (Eu_1 site) with sample M-20 excited at 355 nm ($E=2$ J/cm^2). Inset: $^5D_1$ level PL decay recorded at 543 nm ($^5D_1 \rightarrow {}^7F_1$ transition). The decay is slightly nonexponential and therefore the $^5D_1$ lifetime value is obtained by integrating the decay over time as follows: $\tau_{\text{eff}} = \int_0^\infty (I(t)/I(0))dt$.

C. Eu PL decay study

PL decay characteristics confirm the difference between Eu_1 and Eu_2 sites as well as the strong similarities between implanted and MBE samples. Figure 6 presents the typical early stage of the Eu $^5D_0 \rightarrow {}^7F_2$ luminescence decay in MBE sample M-20 recorded at 620.2 and 622.4 nm. As mentioned previously, these wavelengths are characteristic of the Eu_{2M} and Eu_{1M} sites, respectively. The reconstruction of the recorded PL spectrum using the spectral signatures of the Eu_{1M} and Eu_{2M} sites indicates that within the experimental conditions of Fig. 6 the luminescence at 620.2 nm is 80% due to Eu_2 ions and the emission at 622.4 nm arises for 85% from Eu_1 ions. Significantly, the same PL decay characteristics have been obtained for each Eu site in all samples whether they are implanted or MBE grown. Time dependent PL of the Eu_1 sites of all implanted and *in situ* samples exhibits a similar build-up stage, while no rise time is recorded for the luminescence of Eu_2 ions. Figure 6 reveals the early stage of the Eu decay characteristic for both sites when recording Eu decays at specific emission wavelengths. A similar result can be obtained by recording the Eu decay at the same emission wavelength but changing the pulsed excitation density as shown in Fig. 7(a) for an implanted sample (I-1300). In a similar manner to what is shown under cw excitation in Fig. 1, a change in the Eu PL spectrum is observed by changing the pulsed excitation density as depicted in Fig. 7(b) for sample I-1300. At low photon flux the PL spectrum is dominated by Eu_2 ions and the corresponding decay recorded at 622.6 nm in Fig. 7(a) does not exhibit any build-up stage. As the photon flux increases, the PL spectrum tends to be dominated by Eu_1 ions and the related decay at the same emission wavelength of 622.6 nm comprises a more and more pronounced build-up stage.

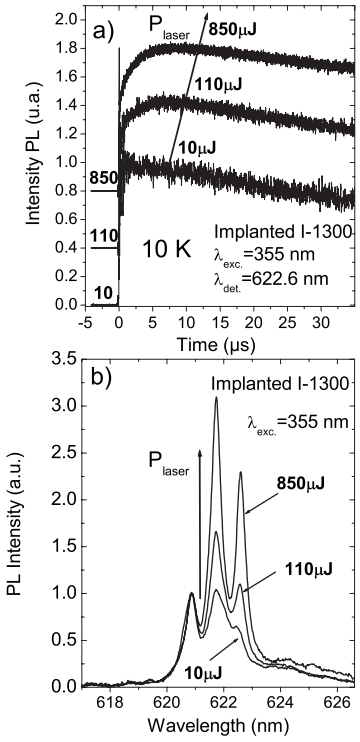

FIG. 7. (a) Initial stage of Eu decay at 622.6 nm under above bandgap excitation at 355 nm in implanted sample I-1300 for three different pulsed excitation densities (10, 110, and 850 μJ) at 10 K; (b) Eu PL spectrum recorded in the same conditions as the Eu decays displayed in (a).

Interestingly, the buildup in Eu_1-related PL dynamics shown in Figs. 6 and 7 does not start from zero. In order to have a better understanding of this build-up phase, all Eu luminescence transients were adjusted with the following equation:

$$I(t) = A_0 e^{-t/\tau_0} + A_1(e^{-t/\tau_0} - e^{-t/\tau_1}), \quad (2)$$

where τ_0 and τ_1 are the $^5D_0$ level decay and build-up time, respectively, A_0 and A_1 are the amplitudes of the two components of the decay (without and with buildup, respectively).

The fitting procedure reveals that the rise time constant τ_1 is about 2.5 μs for all samples. This rise time is likely due to the fact that some Eu_1 ions are first excited to the $^5D_1$ upper level and then relaxed nonradiatively by multiphonon emission to the emitting $^5D_0$ level. This indication of an intermediate step through the $^5D_1$ level is confirmed by the $^5D_1$ level PL decay recorded directly at 543 nm ($^5D_1 \rightarrow {}^7F_1$ transition) under above bandgap excitation. As shown in the inset of Fig. 6, the $^5D_1$ level PL signal decays with a time constant of $\sim$2.5 μs in all samples. Furthermore, the $^5D_1 \rightarrow {}^7F_1$ PL spectrum is nearly identical in all samples and does not change with the photon flux, indicating that only one type of Eu site (Eu_1) emits from the $^5D_1$ level under above bandgap excitation. It is possible that the excitation does not go directly into the $^5D_1$ level but rather to even higher levels such as $^5D_2$ or even $^5D_3$ before relaxing to the $^5D_1$ level and then the $^5D_0$ level.[27] This hypothesis was difficult to confirm because the luminescence arising from the $^5D_2$ and $^5D_3$ levels was too weak to enable a proper lifetime measurement. However, the PL spectrum under above bandgap cw excitation exhibits weak transitions from the $^5D_2$ level suggesting that part of the excitation path could involve the $^5D_2$ level as an intermediate step.

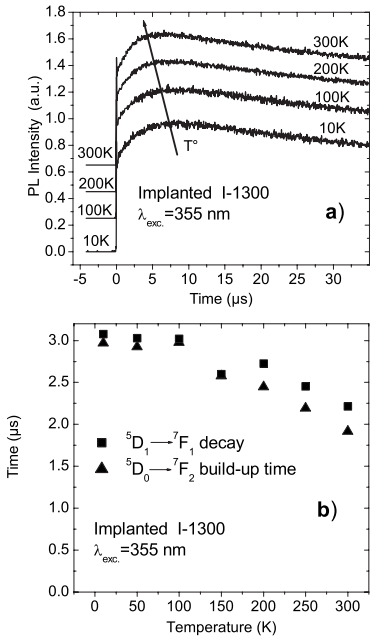

FIG. 8. (a) Initial stage of Eu decay at 622.6 nm as a function of temperature from 10 to 300 K in implanted sample I-1300; (b) comparison between the build-up time of the $^5D_0$ level decay and the $^5D_1$ level decay recorded at 543 nm ($^5D_1 \rightarrow {}^7F_1$ transition) as a function of temperature.

The fact that the build-up phase in Eu_1-related PL dynamics shown in Figs. 6 and 7 does not start from zero indicates that two excitation pathways populate the Eu_1 $^5D_0$ level, one being via the $^5D_1$ level and the other promoting Eu_1 ions directly into the $^5D_0$ level. This result can be explained by keeping in mind that the energy transfer between a bound exciton and a europium ion depends on the spectral overlap between the emission band of the "donor" (bound exciton) and the absorption band of the "acceptor" (europium ion).[28] The emission band of the donor can be broad enough to spectrally overlap with the $^7F_0 \rightarrow {}^5D_J$ absorption bands (J=0, 1 and possibly 2, 3) thus enabling direct energy transfer toward both $^5D_0$ and $^5D_1$ levels. On the other hand, the absence of a rise time in the Eu_2 time dependent $^5D_0 \rightarrow {}^7F_2$ PL shows that the Eu_2 ions unlike Eu_1 ions are not excited into the $^5D_1$ level but only directly into the $^5D_0$ level. Therefore, one could think that in case of Eu_2 ions the spectral overlap between the emission band of the bound exciton and the $^7F_0 \rightarrow {}^5D_1$ absorption band is negligible.

Figure 8(a) shows the temperature dependence of the Eu_1 PL dynamics in implanted sample I-1300 going from 10 up to 300 K. The PL dynamics barely change over the studied range of temperature, meaning that the relative efficiency of both excitation paths (via $^5D_1$ and directly to $^5D_0$) remains unchanged with temperature. The only temperature dependent feature is the build-up time constant [τ_1 in Eq. (2)], which slightly decreases with temperature from about 2.5 μs at 10 K to 1.8 μs at 300 K. As expected, this diminution of the build-up time follows the decrease in the $^5D_1$

TABLE III. Eu $^5D_0$ PL lifetime at 10 K and RT. Some decays exhibit nonexponential features. Therefore, data represent effective lifetime values obtained by integrating the decay over time as follows: $\tau_{\text{eff}}=\int_0^\infty (I(t)/I(0))dt$. In some samples, the Eu_2 $^5D_0$ lifetime could not be extracted in a reliable manner because of a predominance of the Eu_1 PL signal.

	Eu_1		Eu_2	
Sample	10 K	300 K	10 K	300 K
I-1000	60 μs	55 μs	⋯	⋯
I-1100	140 μs	115 μs	⋯	⋯
I-1200	190 μs	175 μs	⋯	⋯
I-1300	220 μs	210 μs	205 μs	100 μs
M-5	260 μs	225 μs	180 μs	75 μs
M-10	270 μs	250 μs	⋯	⋯
M-20	210 μs	205 μs	220 μs	210 μs

level lifetime shown in Fig. 8(b), which is due to an increase in the multiphonon relaxation rate from $^5D_1$ to $^5D_0$ with temperature.

Another interesting result is that the Eu_1 $^5D_0$ level lifetime barely changes with temperature as illustrated in Table III which gives the Eu $^5D_0$ level lifetimes obtained at 10 and 300 K for some samples. Therefore, possible nonradiative decay channels such as temperature activated back transfer from excited Eu_1 ions toward the carrier trap can be considered as small unlike Eu_2 ions for which the $^5D_0$ level lifetime is divided by a factor 2 between 10 and 300 K (Table III). This thermal stability of the Eu_1 red PL decay is a remarkable feature which can be seen in most samples while the Eu_1 red PL intensity itself exhibits various thermal quenching for each sample. In the samples used in this study the $^5D_0 \rightarrow {}^7F_2$ integrated PL intensity under above bandgap excitation ranges from 0.7 to 0.15 at 300 K when assuming unity at 10 K. These differences between samples illustrate the occurrence of thermally activated nonradiative processes which prevent the excitation of substitutional Eu_1 ions which are still excited at low temperature. These nonradiative processes are even stronger for Eu_2 ions, which in most samples barely emit at 300 K. Among such kind of processes one can imagine, for instance, electron or hole emission, which dissociate the electron-hole pair and thus stop the excitation path toward Eu ions.

Table III also shows that the Eu_1 $^5D_0$ level lifetime, while remaining unaffected by temperature, does change among samples, the largest value being 270 μs at 10 K in sample M-10. The range of $^5D_0$ level lifetime values shown in Table III is most likely due to the crystalline quality of each sample. For instance, in implanted samples, as the annealing temperature is raised from 1000 to 1300 °C the $^5D_0$ level lifetime steadily increases from 60 to 220 μs. The main impact of the annealing temperature is to remove defects which otherwise act as luminescence quenching centers. Energy transfer processes from excited Eu ions toward these defects can explain the nonradiative de-excitation which is observed in the Eu $^5D_0$ level decay. Furthermore, it is worth noticing that these nonradiative processes in most cases give rise to nonexponential $^5D_0$ decays. Besides, these quenching mechanisms make it difficult to estimate the $^5D_0$ level radiative lifetime, which otherwise should be fairly easy to assess since no multiphonon relaxation from the $^5D_0$ level is expected. Fortunately, a value of the Eu_1 $^5D_0$ level radiative lifetime can be derived by looking at the ratio of the $^5D_0 \rightarrow {}^7F_1$ transition intensity to the total $^5D_0 \rightarrow {}^7F_J$ intensity. The $^5D_0 \rightarrow {}^7F_1$ transition is a magnetic dipole transition and therefore its strength can be considered as constant regardless of the environment and calculated from theoretical considerations. The $^5D_0$ level radiative lifetime τ_r can then be derived as follows:[29]

$$\frac{1}{\tau_r} = A_{\text{tot}} = I_{\text{tot}}\left(\frac{A_{\text{MD},0} \times n^3}{I_{\text{MD}}}\right), \tag{3}$$

where n is the refractive index of the medium, $A_{\text{MD},0}$ is the magnetic dipole $^5D_0 \rightarrow {}^7F_1$ transition rate in vacuum, I_{tot} and I_{MD} are the integrated intensities of the $^5D_0 \rightarrow {}^7F_J$ bands and the $^5D_0 \rightarrow {}^7F_1$ band, respectively. Equation (3) makes use of the fact that magnetic dipole transition rates can be calculated and be used as a transition rate "scaling" for other transitions. It has been shown that Eq. (3) gives very good results in the case of europium in predicting the $^5D_0$ radiative lifetime in various hosts.[29] Using a value of 14.65 s^{-1} for $A_{\text{MD},0}$ (Ref. 29) and 2.4 for the GaN refractive index at 620 nm, we derived a value of 430 μs for the $^5D_0$ level radiative lifetime in GaN. This value, when compared to the 270 μs $^5D_0$ lifetime measured at 10 K in sample M-10, suggests that at least 37% of Eu_1 ions actually decay via nonradiative processes.

D. Eu doped GaN QDs

A similar study was performed with Eu doped GaN QDs. Above bandgap excitation was performed at 325 (HeCd laser) or 266 nm (quadrupled-Nd:YAG pulsed laser) and gave similar PL results, the GaN QD bandgap edge lying between 380 and 420 nm. The redshift with respect to GaN bandgap is due to the large height of the dots[21] and to the concomitant quantum confined Stark effect, which results from the very large internal electric field, commonly observed in GaN/AlN heterostructures.[30] As displayed in Fig. 9(a) under above bandgap excitation, the same type of build-up stage was observed due to the $^5D_1$ level acting as an intermediate step in the $^5D_0$ level filling as in implanted and MBE samples. However, no direct $^5D_0$ decay, as reported for Eu_2 ions, could be observed even when trying to monitor the Eu decay at different emission wavelengths as shown in Fig. 6 or when changing the excitation density, as reported in Fig. 7. This absence of change in the decay strongly suggests that only one type of Eu site is excited under above bandgap excitation. In a similar manner no PL spectrum change could be recorded by changing the excitation energy density. The typical PL spectrum obtained in Eu doped GaN QDs under above bandgap excitation at 266 nm is displayed in Fig. 9(b). This nonresonant PL spectrum consists of a broad line while the resonant spectrum excited at 471 nm also shown in Fig. 9(b) encompassing all Eu ions consists of a more resolved spectrum which resembles the Ga substitutional Eu ion signature displayed in Fig. 3. The fact that the Eu spectra under resonant and nonresonant excitations are different suggests that, similarly to implanted or MBE samples, the vast major-

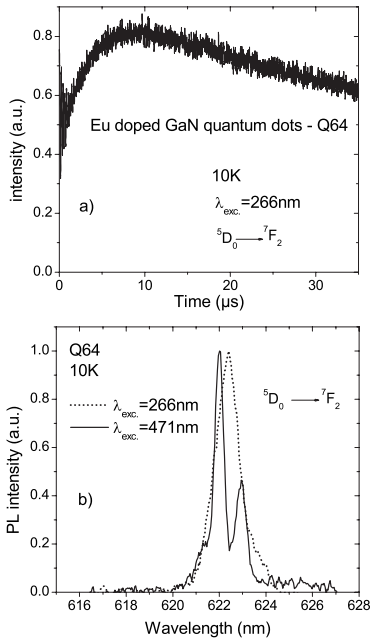

FIG. 9. (a) Initial stage of Eu decay at 622.5 nm in Eu doped GaN QDs at 10 K following an above bandgap excitation at 266 nm; (b) comparison between Eu spectrum under above bandgap excitation (λ_{exc}=266 nm) and under resonant excitation at 471 nm ($^7F_0 \rightarrow {}^5D_2$ transition) in Eu doped GaN QDs.

ity of Eu ions are located in Ga substitutional sites and cannot be excited nonresonantly. On the other hand, the Eu resonant and nonresonant spectra in Fig. 9(b) also share similarities as the center emission wavelength is the same for both spectra. The larger spectral broadening observed for Eu ions excited nonresonantly at 266 nm is most likely due to inhomogeneous strains within the GaN QDs involved in the Eu nonresonant excitation process. All these remarks suggest that Eu ions excited at 266 nm through GaN QD bear similarities with Eu_1 ions as they exhibit a similar build-up stage and the same center emission wavelength as Eu ions located in Ga susbtitutional sites. However, the large inhomogeneous broadening of their PL spectrum indicates that these Eu ions occupy local sites within a large variety of distorted Ga substitutional sites.

Looking in more details at the PL dynamics one can notice that the Eu time dependent PL in Eu doped QDs is not strictly identical to what is observed in implanted and MBE samples. The main difference lies in the ratio between the two excitation paths (directly to $^5D_0$ level or via $^5D_1$ level) which can be described by the ratio A_1/A_0+A_1 derived from the fitting procedure using Eq. (2). This ratio represents the relative part of the excitation mechanism mediated by the $^5D_1$ level compared to both excitation paths. The A_1/A_0+A_1 ratios are equal to 0.35 and 0.36 for implanted and MBE samples, respectively, while it reaches 0.54 for Eu doped GaN QDs. The excitation pathway going through the $^5D_1$ level clearly plays a more important role in Eu doped GaN QDs than in the other types of samples. This difference could again be explained by a difference in the spectral overlap between the emission band of the donors (bound excitons) and the absorption band of the acceptors (europium ions) which in Eu doped GaN QD would favor a direct energy transfer toward the $^5D_1$ level.

IV. CONCLUSION

A similar change with above bandgap excitation flux level is observed in the high-resolution spectra of the Eu $^5D_0 \rightarrow {}^7F_2$ transition for Eu implanted and Eu *in situ* doped MBE samples, grown and doped in different laboratories. This change is explained by PL contributions from two distinct Eu sites, namely, Eu_1 and Eu_2, with Eu_2 ions being more efficiently excited via the host matrix than Eu_1 ions. The Eu_{1I} and Eu_{1M} spectra are very similar in implanted and MBE samples, whereas Eu_{2I} and Eu_{2M} have different PL spectra. The similarity between Eu_1 spectra and resonant spectra in both types of samples indicate that Eu_1 ions occupy Ga substitutional sites. PL saturation experiments also reveal that the concentrations of Eu_1 and Eu_2 ions are of the same order of magnitude and only represent a small part of the majority of Eu ions which are located in Ga substitutional sites and cannot be excited through the GaN host. The luminescence from Eu_1 ions exhibits a rise time of 2.5 μs at 10 K attributed to the decay from the upper $^5D_1$ level to the emitting $^5D_0$ level in both implanted and MBE samples. The Eu_2 luminescence does not exhibit this rise time which suggests that Eu_2 ions are directly excited into the $^5D_0$ level. The direct excitation of Eu ions into the $^5D_0$ emitting level is also observed for Eu_1 ions. These results suggest that a spectral overlap between the emission spectrum of a nearby bound exciton and the $^7F_0 \rightarrow {}^5D_0$ absorption band exists for both Eu_1 and Eu_2 ions, while a spectral overlap with the $^7F_0 \rightarrow {}^5D_J$ (J=1 and possibly 2, 3) absorption band occurs only for Eu_1 ions. Under above bandgap excitation, the relative efficiency of both Eu_1 excitation mechanisms (mediated by the $^5D_1$ level or directly to the $^5D_0$ level) remains stable with temperature suggesting that temperature does not affect the spectral overlaps involved in the two energy transfers.

A tentative conclusion is that Eu_1 ions in both MBE and implanted samples occupy Ga substitutional sites with a carrier trap located in the second or third neighboring shell, while Eu_2 ions are located on a site distorted by a much closer local defect, which is electrically active as a carrier trap. The close proximity of the carrier trap to the Eu_2 ions explains the higher excitation efficiency of this Eu center in comparison to Eu_1 ions. The lattice distortion introduced by the local defect close to Eu_2 ions is not the same in implanted and *in situ* doped samples giving rise to a different PL spectrum. Eu luminescence in Eu doped GaN QDs exhibits similarities with Eu_1 ion spectroscopic features observed both in implanted and *in situ* doped GaN samples. However, the broad Eu PL spectrum indicates that Eu ions in GaN QDs occupy distorted Ga substitutional sites.

The multiplicity of RE incorporation sites can be detrimental for light-emitting diode or laser applications since it implies that different excitation paths lead to different emitting centers. In contrast, an efficient device would require that the majority of RE ions occupy a similar site with a high excitation efficiency. In this sense, incorporation sites such as Eu_2 ions should be favored and specifically expanded through defect engineering.

ACKNOWLEDGMENTS

This work was supported by the European Research Training Network Project RENiBEl (Contract No. HPRN-CT-2001-00297) and by the CEA (French Atomic Energy Center) which provides the PhD fellowship of one of us (L.B.). The work at Cincinnati was supported in part by the U.S. Army Research Office (Grant No. DAAD19-03-1-0101). The authors acknowledge the support, encouragement, and many technical discussions with J. M. Zavada. Fruitful discussions with Dr. B. Gayral are also acknowledged regarding the Eu doped GaN QDs.

[1] *Proceedings of E-MRS Symposium, 2003*, edited by P. Ruterana [Mater. Sci. Eng., B **105**, 1 (2003)]
[2] A. J. Steckl, J. C. Heikenfeld, D. S. Lee, M. J. Garter, C. C. Baker, Y. Wang, and R. Jones, IEEE J. Sel. Top. Quantum Electron. **8**, 749 (2002).
[3] J. H. Park and A. J. Steckl, Appl. Phys. Lett. **85**, 4588 (2004).
[4] J. H. Park and A. J. Steckl, J. Appl. Phys. **98**, 056108 (2005).
[5] J. C. Heikenfeld, M. Garter, D. S. Lee, R. Birkhahn, and A. J. Steckl, Appl. Phys. Lett. **75**, 1189 (1999).
[6] H. J. Lozykowski, W. M. Jadwisienczak, J. Han, and I. G. Brown, Appl. Phys. Lett. **77**, 767 (2000).
[7] E. E. Nyein, U. Hömmerich, J. Heikenfeld, D. S. Lee, A. J. Steckl, and J. M. Zavada, Appl. Phys. Lett. **82**, 1655 (2003).
[8] H. Y. Peng, C. W. Lee, H. O. Everitt, D. S. Lee, A. J. Steckl, and J. M. Zavada, Appl. Phys. Lett. **86**, 051110 (2005).
[9] H. Bang, S. Morishima, Z. Li, K. Akimoto, M. Nomura, and E. Yagi, J. Cryst. Growth **237–239**, 1027 (2002).
[10] A. M. Mitofsky, G.C. Papen, S. G. Bishop, D.S. Lee, and A. J. Steckl, Mater. Res. Soc. Symp. Proc. **639**, G6.26 (2001).
[11] U. Hommerich, J. T. Seo, C. R. Abernathy, A. J. Steckl, and J. M. Zavada, Mater. Sci. Eng., B **81**, 116 (2001).
[12] S. Kim, R. L. Henry, A. E. Wickenden, D. D. Koleske, S. J. Rhee, J. O. White, J. M. Young, K. Kim, X. Li, J. J. Coleman, and S. G. Bishop, J. Appl. Phys. **90**, 252 (2001).
[13] K. Lorenz, U. Wahl, E. Alves, S. Dalmasso, R. W. Martin, K. P. O'Donnell, S. Ruffenach, and O. Briot, Appl. Phys. Lett. **85**, 2712 (2004).
[14] L. Bodiou, A. Oussif, A. Braud, J.-L. Doualan, R. Moncorgé, K. Lorenz, and E. Alves, Opt. Mater. (Amsterdam, Neth.) **28**, 780 (2006).
[15] K. Wang, R. W. Martin, K. P. O'Donnell, V. Katchkanov, E. Nogales, K. Lorenz, E. Alves, S. Ruffenach, and O. Briot, Appl. Phys. Lett. **87**, 112107 (2005).
[16] E. E. Nyein, U. Hömmerich, C. Munasinghe, A. J. Steckl, and J. Zavada, Mater. Res. Soc. Symp. Proc. **866**, 67 (2005).
[17] H. Peng, C. W. Lee, H. O. Everitt, C. Munasinghe, D. S. Lee, and A. J. Steckl, J. Appl. Phys. **102**, 073520 (2007).
[18] H. Park and A. J. Steckl, Appl. Phys. Lett. **88**, 011111 (2006).
[19] C. Munasinghe and A. J. Steckl, Thin Solid Films **496**, 636 (2006).
[20] C. Munasinghe, A. J. Steckl, E. E. Nyein, U. Hömmerich, H. Peng, H. Everitt, Z. Fleischman, V. Dierolf, and J. Zavada, Mater. Res. Soc. Symp. Proc. **866**, 41 (2005).
[21] Y. Hori, F. Enjalbert, E. Monroy, D. Jalabert, L. S. Dang, X. Biquard, M. Tanaka, O. Oda, and B. Daudin, Appl. Phys. Lett. **84**, 206 (2004).
[22] K. Takahei, A. Taguchi, H. Nakagome, K. Uwai, and P. S. Whitney, J. Appl. Phys. **66**, 4941 (1989).
[23] J.-S. Filhol, R. Jones, M. J. Shaw, and P. R. Briddon, Appl. Phys. Lett. **84**, 2841 (2004).
[24] U. Wahl, E. Alves, K. Lorenz, J. G. Correia, T. Monteiro, B. De Vries, A. Vantomme, and R. Vianden, Mater. Sci. Eng., B **105**, 132 (2003).
[25] K. C. Mishra, V. Eyert, and P. C. Schmidt, Z. Phys. Chem. **221**, 1663 (2007).
[26] A. Braud, J. L. Doualan, R. Moncorgé, B. Pipeleers, and A. Vantomme, Mater. Sci. Eng., B **105**, 101 (2003).
[27] C. W. Lee, H. O. Everitt, D. S. Lee, A. J. Steckl, and J. M. Zavada, J. Appl. Phys. **95**, 7717 (2004).
[28] D. L. Dexter, J. Chem. Phys. **21**, 836 (1953).
[29] M. H. Werts, R. T. F. Jukes, and J. W. Verhoeven, Phys. Chem. Chem. Phys. **4**, 1542 (2002).
[30] J. Simon, N. T. Pelekanos, C. Adelmann, E. Martinez-Guerrero, R. André, B. Daudin L. S. Dang, and H. Mariette, Phys. Rev. B **68**, 035312 (2003).